IN-02
84437
P-12

NASA Technical Memorandum 107576

FURTHER INVESTIGATIONS OF THE AEROELASTIC BEHAVIOR OF THE AFW WIND-TUNNEL MODEL USING TRANSONIC SMALL DISTURBANCE THEORY

WALTER A. SILVA
ROBERT M. BENNETT

MARCH 1992

National Aeronautics and
Space Administration

Langley Research Center
Hampton, Virginia 23665

(NASA-TM-107576) FURTHER INVESTIGATIONS OF THE AEROELASTIC BEHAVIOR OF THE AFW WIND-TUNNEL MODEL USING TRANSONIC SMALL DISTURBANCE THEORY (NASA) 12 p CSCL 01A
N92-22240
Unclas
G3/02 0084437

FURTHER INVESTIGATIONS OF THE AEROELASTIC BEHAVIOR OF THE AFW WIND-TUNNEL MODEL USING TRANSONIC SMALL DISTURBANCE THEORY

Walter A. Silva and Robert M. Bennett
Unsteady Aerodynamics Branch
NASA Langley Research Center
Hampton, VA 23665-5225

ABSTRACT

The CAP-TSD (Computational Aeroelasticity Program - Transonic Small Disturbance) code, developed at the NASA Langley Research Center, is applied to the Active Flexible Wing wind-tunnel model for prediction of transonic aeroelastic behavior. A semi-span computational model is used for evaluation of symmetric motions, and a full-span model is used for evaluation of antisymmetric motions. Static aeroelastic solutions using CAP-TSD are computed. Dynamic (flutter) analyses then are performed as perturbations about the static aeroelastic deformations and presented as flutter boundaries in terms of Mach number and dynamic pressure. Flutter boundaries that take into account modal refinements, vorticity and entropy corrections, antisymmetric motions and sensitivity to the modeling of the wing tip ballast stores also are presented and compared with experimental flutter results.

INTRODUCTION

An understanding of the aeroelastic behavior of flight vehicles in the transonic Mach number regime is of great importance for flight safety. For example, it is well known that aircraft flying into or through the transonic regime may encounter a region of reduced flutter speed known as the transonic flutter dip. Valuable insight into the nature of this transonic flutter dip phenomenon is provided by Isogai[1] for a typical, two-dimensional streamwise section of an aft-swept wing, while comparison of aerodynamic predictions with the experiments reported by Davis and Malcolm[2] reveals the limitations of linear theory when applied in the transonic regime. Linear aerodynamic predictions, although highly successful in the subsonic and supersonic regimes, normally cannot be used to predict transonic aeroelastic behavior accurately. Transonic flow equations capable of modeling flow nonlinearities (shocks, boundary layer, separation and vorticity) and boundary conditions that induce nonlinear effects (airfoil thickness and shape, and large deflections) then must be solved. The surveys by Edwards and Malone[3] and Ballhaus and Bridgeman[4] review developments in the field of computational transonic aeroelasticity. Some of these developments include modeling of the Navier-Stokes equations[5] and the Euler equations[6] for flutter analysis. Application of these higher order formulations to complete aircraft configurations have been limited due to the large computational resources required. Certain assumptions regarding the flow that results in reduced-order formulations such as the full potential equation[7] and the computationally efficient transonic small-disturbance (TSD) equation can be made. Research efforts involving the TSD formulation include the development of the XTRAN3S code,[8] the work by Yang, Guruswamy, and Striz,[9] and many others.

A transonic aeroelasticity code known as CAP-TSD (Computational Aeroelasticity Program-Transonic Small Disturbance) was developed at the NASA Langley Research Center (LaRC). CAP-TSD is capable of analysis of configurations that have multiple lifting surfaces with control surfaces, bodies (nacelles, stores), vertical surfaces, and a fuselage and solves the TSD equation using an efficient approximate factorization scheme.[10] References 11 and 12 verified the ability of the code to predict steady and unsteady pressures accurately for wings and configurations at subsonic, transonic, and supersonic Mach numbers. Flutter prediction using CAP-TSD for two thin, swept and tapered wings compared well with experimental flutter results.[13]

The goal of the present study was to update the transonic aeroelastic analysis of the Active Flexible Wing (AFW) wind-tunnel model[14] that was reported in Ref. 15. The AFW model (Fig. 1) is a full-span, sting-mounted wind-tunnel model designed and built by the Rockwell International Corporation. The main goal of the AFW program was to design, implement and validate digital control laws for flutter suppression[14] which could operate simultaneously with rolling maneuver control laws. Therefore, knowledge of possible regions of instability was desirable.

ORIGINAL PAGE
BLACK AND WHITE PHOTOGRAPH

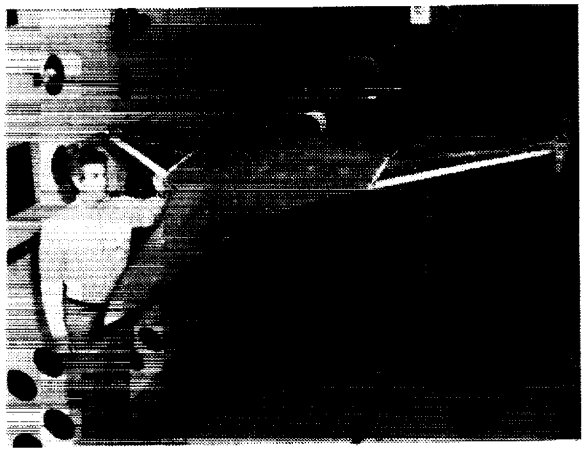

Fig. 1 Model mounted in the Langley Transonic Dynamics Tunnel.

This paper first presents the computational procedures contained in CAP-TSD. This includes a brief description of the TSD formulation and the coupled aerodynamic and structural equations of motion that are integrated in time. These equations were used for static and dynamic aeroelastic analyses of the AFW wind-tunnel model. An important conclusion of studies by Yates, Wynne, and Farmer[16] and Yates and Chu[17] was that the accuracy of the transonic flutter prediction is highly dependent on the accuracy of the static aeroelastic state of the wing. As a result, a procedure for computing static aeroelastic deformations[15] was applied to the AFW computational model. The dynamic behavior was computed as a perturbation about previously computed static aeroelastic solutions. The resultant dynamic time histories of the generalized displacements then were analyzed using a modal identification technique to estimate the stability parameters (damping and frequency) of the system at a given Mach number and dynamic pressure. Dynamic results are presented in the form of flutter boundaries, in terms of Mach number and flutter dynamic pressure. Flutter boundaries that account for corrected modeling of the wing tip ballast store of the AFW wind-tunnel model (corrected the modeling in Ref. 15), updated mode shapes and frequencies, and vorticity and entropy corrections, and a subsonic antisymmetric flutter result are presented and compared with experimental flutter results.

COMPUTATIONAL PROCEDURES

In this section, an overview of the computational procedures including a description of the CAP-TSD code, the aeroelastic equations of motion, the time-marching solution of these equations, and the modal identification of the resulting free decay transients are presented.

TSD Equation

The CAP-TSD code is a finite-difference program which solves the general-frequency modified TSD potential equation

$$M_\infty^2 (\phi_t + 2\phi_x)_t = [(1 - M_\infty^2)\phi_x + F\phi_x^2 + G\phi_y^2]_x + (\phi_y + H\phi_x\phi_y)_y + (\phi_z)_z \qquad (1)$$

where M_∞ is the freestream Mach number, ϕ is the disturbance velocity potential, and the subscripts of ϕ represent partial derivatives.

Several choices are available for the coefficients F, G, and H depending upon the assumptions used in deriving the TSD equation. For current applications, the coefficients are defined as

$$F = -\frac{1}{2}(\gamma + 1) M_\infty^2 ,$$

$$G = \frac{1}{2}(\gamma - 3) M_\infty^2 ,$$

$$H = -(\gamma - 1) M_\infty^2 \qquad (2)$$

where γ is the ratio of specific heats. The linear potential equation is recovered simply by setting F, G, and H equal to zero.

Equation (1) is solved within CAP-TSD by a time-accurate approximate factorization (AF) algorithm developed by Batina.[10] In Refs. 11 to 13, the AF algorithm was shown to be efficient for application to steady or unsteady transonic flow problems. It can provide accurate solutions in only several hundred time steps yielding a significant computational cost savings when compared to alternative methods.

Several algorithm modifications have been made which improve the stability of the AF algorithm and the accuracy of the results.[18,19] Two of these improvements are vorticity and entropy corrections[19] for improved shock modeling. The effect of these corrections on the transonic flutter boundary of the AFW wind-tunnel model was investigated and is presented in a subsequent section of this paper.

The CAP-TSD program can be used for analysis of configurations with combinations of lifting surfaces and bodies including canard, wing, tail, control surfaces, tip launchers, pylons, fuselage, stores, and nacelles. The configuration capability of the current version of CAP-TSD permits the calculation of pressures on the fuselage and bodies. In this version however, modal perturbations of the fuselage and bodies were not included in the boundary conditions and the integration of the pressures on the fuselage and on bodies (for computation of the generalized aerodynamic forces) was not included in the aeroelastic solution. However, the aerodynamic influence of the fuselage and the wing tip body of the AFW wind-tunnel model were included as interference effects upon the wing pressures.

Equations of Motion

The aeroelastic equations of motion are based on a right-hand orthogonal coordinate system with the x-direction defined as positive downstream, y-direction positive out the right wing, and the z-direction positive upward. The equations of motion may be written as

$$M\ddot{q} + C\dot{q} + Kq = Q \qquad (3)$$

where q is a vector of generalized displacements, M is the generalized mass matrix, C is the generalized damping matrix, and K is the generalized stiffness matrix. Q is the vector of generalized forces where its elements are defined as

$$Q_i = \frac{\rho U^2}{2} c_r^2 \int_s \frac{\Delta p\, h_i}{\rho U^2/2} \frac{dS}{c_r^2}$$

Δp is the lifting pressure, ρ is the fluid density, c_r is the root chord, U is the freestream velocity, S is the area of the lifting surface(s) and h_i is the vibration mode shape. Equation (3) is rewritten as

$$\ddot{q} = -M^{-1} Kq - M^{-1} C\dot{q} + M^{-1} Q \qquad (4)$$

to permit integration of the equation with respect to time.

Time-Marching Aeroelastic Solution

The aeroelastic solution procedure implemented within CAP-TSD for integrating Eq. (4) is similar to that described by Edwards, Bennett, Whitlow, and Seidel.[20] Equation (4) is composed of normal mode equations which may be expressed in linear, first-order state-space form as

$$\dot{x}_i = Ax_i + Bu_i \qquad (5)$$

where

$$x_i = [\, q_i \;\; \dot{q}_i \,]^T$$

and

$$A = \begin{bmatrix} 0 & 1 \\ -m_i^{-1} k_i & -m_i^{-1} c_i \end{bmatrix}$$

$$B = m_i^{-1} \frac{\rho U^2}{2} c_r^2 \begin{bmatrix} 0 \\ 1 \end{bmatrix}$$

$$u_i = \int_s \Delta C_p\, h_i\, dS/c_r^2$$

$$\Delta C_p = \frac{\Delta p}{\rho U^2/2}$$

In these definitions, m_i, c_i, and k_i are elements of the mass, damping, and stiffness matrices, respectively, corresponding to mode i. The analytical solution to Eq. (5) is found in Ref. 20 and a description of its numerical implementation in CAP-TSD is found in Ref. 13.

For aeroelastic analysis, two steps generally are required in performing the calculations. In the first step, the steady-state flow field is calculated to account for wing thickness, camber, mean angle of attack, and static aeroelastic deformation, thus providing the starting flow field for the dynamic aeroelastic analysis. Previously published CAP-TSD flutter studies, with the exception of Ref. 15, analyzed only symmetric wings at zero steady angle of attack[13], thereby avoiding the problem of static aeroelastic deformations. For the AFW wind-tunnel model, the airfoil sections are not symmetric and the wing has twist. Thus a procedure for computing static aeroelastic solutions had to be developed before an accurate dynamic analysis could be performed. The dynamic analysis then would be a perturbation about a converged static aeroelastic solution at each Mach number and dynamic pressure of interest.

The procedure developed[15] and applied in this study for computing static aeroelastic deformations is to allow the structure and aerodynamics to interact with no initial excitation (no initial deflection or velocity) and with a large value of viscous damping to prevent divergence of the solution. This method resulted in convergence of the generalized displacements. Static aeroelastic deformations should be independent of viscous damping and therefore different values of viscous damping (ζ=.375, .707, and .99) were evaluated. A typical result for this type of analysis is presented in Fig. 2, which shows a representative variation of a generalized displacement as a function of computational time steps for the three values of viscous damping. It is clear from Fig. 2 that the generalized displacements converged to a value that is independent of the value of viscous damping. Furthermore, the larger the value of viscous damping, the faster the convergence. Therefore, the highest value of viscous damping (ζ = 0.99) was used in order to accelerate the static aeroelastic solution. For the applications presented herein, 2000 to 4000 time steps were used to converge the static aeroelastic solutions.

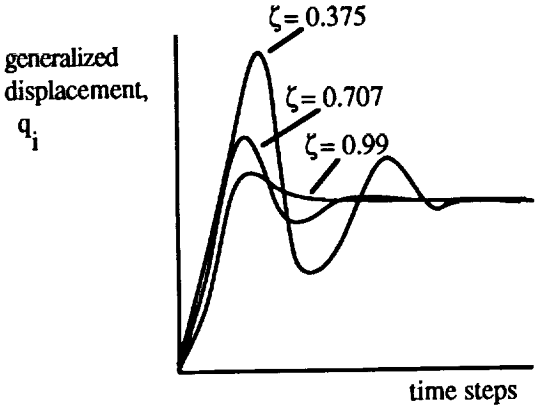

Fig. 2 Convergence of generalized displacements for different values of viscous damping.

An interesting result of this procedure was that it allowed the computation of static aeroelastic deformations at dynamic pressures above the flutter dynamic pressure for the AFW wind-tunnel model. Once converged static aeroelastic solutions were computed, the next step was to prescribe an initial disturbance to begin the dynamic structural integration. Modal velocities in the first three modes were used as initial perturbations. Approximately 7 cycles of the lowest frequency (first) mode were needed for accurate modal identification. For a constant, non-dimensional time step of 0.01, this required 8000 time steps. In determining a flutter point, the freestream Mach number, M_∞, and the associated freestream speed, U, were held fixed. A value of the dynamic pressure, $q = \rho U^2/2$, then was used, and free decay transients were computed. These resulting transients of the generalized coordinates were analyzed for their content of damped or growing sine-waves, with the rates of decay or growth indicating whether the dynamic pressure was above or below the flutter value. This indicated whether to increase or decrease the value of dynamic pressure in subsequent analyses to determine a neutrally stable result.

Modal Identification

As previously mentioned, CAP-TSD generates free decay transients that must be analyzed for the modal stability characteristics. A typical transient for the AFW model, calculated using CAP-TSD is shown in Fig. 3(a).

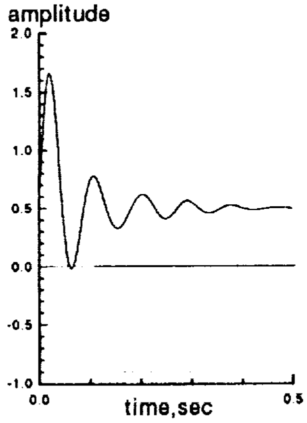

(a) aeroelastic transient.

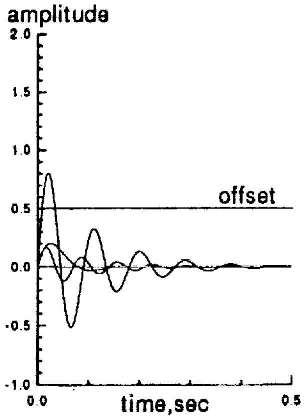

(b) offset and identified modal components.

Fig. 3 Example of modal identification.

The first three modes used in the analysis were excited by specifying an initial condition for each modal velocity to produce a complex decay record. This record is analyzed using a least-squares curve-fit of the response data with complex exponential functions. The program utilized is a derivative of the one described in Ref. 21. The components of the transient of Fig. 3(a) are plotted in Fig. 3(b) to the same scale. The free decay properties of each mode for this condition are readily apparent and the mean or offset value is the static aeroelastic deformation of the mode being analyzed. A sufficient range of dynamic pressure must be considered to determine all relevant flutter points.

ANALYSIS AND RESULTS

CAP-TSD Computational Model

The AFW geometry data, including detailed airfoil shape information, was obtained from Rockwell International. From this geometry data, two computational models were generated. A half-span model, with a vertical plane of symmetry specified at the centerline, was used for symmetric analyses, and a full-span model was used for antisymmetric analyses. Both computational models consisted of a fuselage, a region aft of the main wing and next to the fuselage referred to as the coat-tail, the main wing(s) with four control surfaces per wing, and the wing tip ballast store(s). The four control surfaces per wing are the leading-edge inboard (LEI), leading-edge outboard (LEO), trailing-edge inboard (TEI), and trailing-edge outboard (TEO). Each control surface has a chord that is 25% of the local chord and a span that is 28% of the semi-span. The airfoil definition includes the control surface actuator bumps on the outboard half of the wing. There are slight surface discontinuities on the wind-tunnel model where the wing box and control surfaces meet (at the quarter- and three-quarter chord). These discontinuities are not included in the analytical model because of potential numerical difficulties. The effect of the actuator bumps and the control surface/wing box discontinuities on the measured and computed static pressure distributions will be presented in a subsequent section.

The grid dimensions for the half-span model are 134x51x62 in the x-, y-, and z-directions respectively for a total of 423,708 grid points. The grid extends 10 root chords upstream, 10 root chords downstream, 2 semi-span lengths in the y-direction, and 10 root chords in the positive and negative z-direction. The full-span grid is dimensioned 134x101x62 grid points in the x-, y-, and z-directions (839,108 grid points). The wind-tunnel sting mount is modeled by extending the computational fuselage aft to the downstream boundary of the grid. The grid density was increased in regions where large changes in the flow were expected, such as at the leading edge, trailing edge, wing tip, and control-surface sides and hinge lines.

A computer-generated image of the CAP-TSD model of the AFW wind-tunnel model is shown in Fig. 4. Although not shown in the figure, a protrusion on the

ORIGINAL PAGE
BLACK AND WHITE PHOTOGRAPH

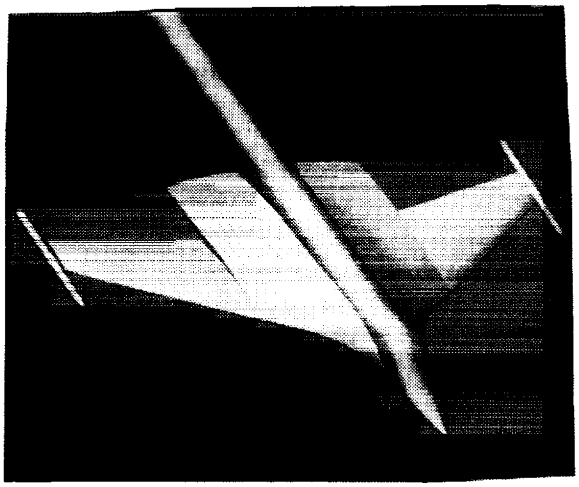

Fig. 4 CAP-TSD computational model of the AFW.

underside of the fuselage that houses the model's pitch actuator is also included in the analytical model.

Analytical modes and frequencies were obtained from a finite-element model, that includes the mass of the tip ballast store, and separated into symmetric and antisymmetric modal data sets. The flutter analyses of Ref. 15 were performed using analytical mode shapes with measured frequencies (from a ground vibration test). Since the symmetric data were shown by linear analysis[14] to be the most flutter critical in the higher, subsonic Mach number regime, only symmetric motions were analyzed in Ref. 15 using the semi-span model. Since then, an updated set of symmetric and antisymmetric mode shapes were generated based on experimental data. These updated mode shapes are defined for a denser set of structural points for improved accuracy in the interpolation procedure. The interpolation of mode shape displacements and slopes at the computational grid points was done via a surface spline.[22] Each structural section was splined separately and then recombined to form the necessary input to CAP-TSD. The separate structural sections are the wing box, coat-tail, and the four control surfaces. Slender bodies such as the fuselage and tip ballast store are not given any modal definition in CAP-TSD, as was previously mentioned. Therefore, no modal data were needed for these components.

Static Results - Pressure distributions

The accuracy of the static aeroelastic solution was investigated in Ref. 15 by comparing analytical results obtained using the original set of symmetric mode shapes with existing experimental data. Two sets of experimental data from previous AFW wind tunnel tests in a heavy gas were used for this purpose. These data included : 1) pressure coefficient distributions and 2) control-surface effectiveness parameters. In Ref. 15, by comparing calculated and experimental pressure distributions at a chosen Mach number and dynamic pressure, it was concluded that the static aeroelastic procedure provided reasonable estimates of the static aeroelastic deformation of the AFW wind-tunnel model using the original set of mode shapes. It also was concluded that comparisons of the calculated and experimental control surface effectiveness parameters were reasonable qualitatively but were deficient quantitatively due to the lack of viscous effects in the CAP-TSD model. Therefore, in the present study, the accuracy of the static aeroelastic procedure is not reassessed, but instead only a comparison of calculated pressure distributions using the updated set of mode shapes and the experimental pressure distributions is presented. The AFW configuration for these previous tests did not include the tip ballast store used in the recent test so that in order for the CAP-TSD calculations to compare with the earlier experiments, the tip ballast store was deleted from the computational model and replaced by a tip fairing.

Figure 5 presents pressure coefficient distributions versus fraction of chord for CAP-TSD with the updated set of mode shapes and experiment at $M_\infty = 0.9$ and a dynamic pressure of 150 psf at the three spanwise stations shown. As with the original set of mode shapes, the

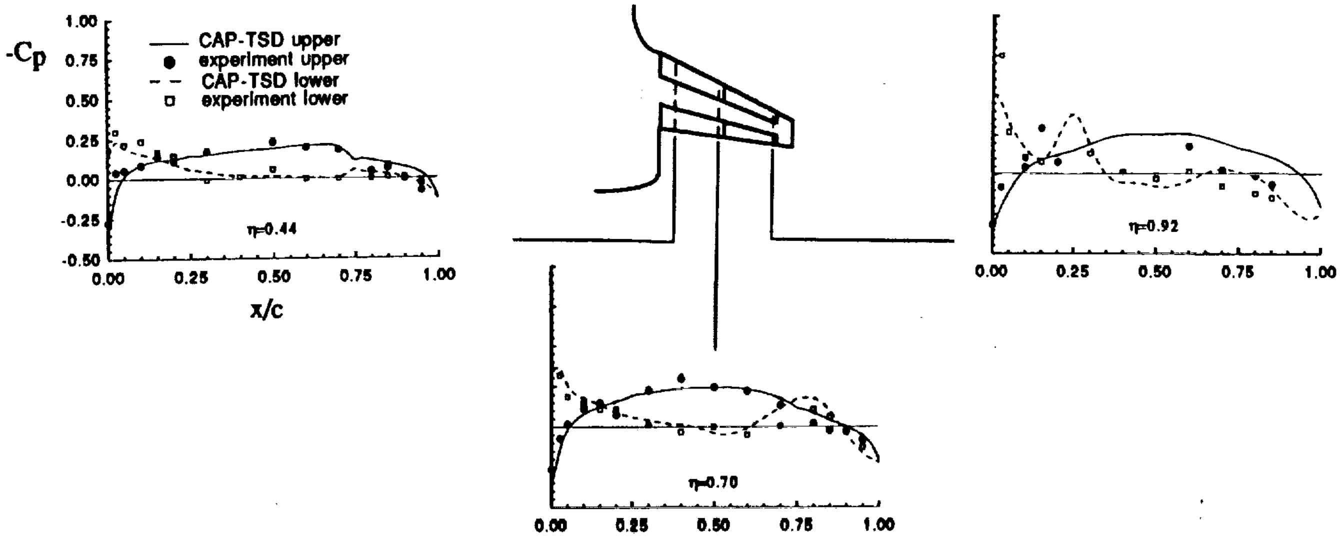

Fig. 5 Pressure distributions at M_∞=0.9 and q=150 psf in a heavy gas.

overall agreement between the most recent analysis and experiment is good, with some discrepancies occurring near the trailing edge and wing tip. The first two span stations compare reasonably well from the leading edge up to about sixty percent of the local chord. Sudden changes in the experimental data can be seen near the quarter-chord at the second span station and near the three-quarter chord for all three span stations. These disruptions in the flow may be caused by the previously-mentioned physical discontinuities where wing box and control surfaces meet. At the second and third span stations, the effect of the actuator bumps on the lower surface pressures is evident. Agreement between analysis and experiment deteriorates at the outboard span station, possibly due to separated and/or tip vortex flow around the wing tip region.

Comparisons of the static aeroelastic results using the updated structural model with those of the previous model of Ref. 15 show essentially the same behavior. There exists a slight difference between the two results at the first span station near the three-quarter chord location where the updated structural model reveals the presence, or beginnings of, a shock that was not present with the original structural model. This appears to be a slight improvement in comparison with the test data. However, the exact cause of the sudden change in the experimental pressure distribution at this location is not clear as it may be due to a shock or to the geometric discontinuity that exists at the quarter-chord and three-quarter chord locations of the wing.

Dynamic Results - Symmetric motions

Flutter dynamic pressures were computed at M_∞=0.5, 0.9, 0.92, 0.93, 0.94, and 0.95. The analyses that included the vorticity and entropy corrections were computed at M_∞=0.5, 0.9, 0.92, 0.93, and 0.95. The original flutter boundary computed prior to the 1989 wind-tunnel test includes a flutter dynamic pressure at M_∞=0.975. Although the results for all of these Mach numbers are included in the figures, results are discussed primarily for the M_∞=0.5, 0.9, 0.93, and 0.95 cases. All flutter analyses are for the AFW model in air at 1.5 degrees angle of attack and include a viscous damping of 0.015 (structural damping of 0.03) for all modes.

In Ref. 15, a rather severe transonic flutter dip was computed using the CAP-TSD code and the bottom of this computational transonic flutter dip did not agree well with experiment. Figure 6, from Ref. 15, is a comparison of the CAP-TSD computed flutter boundary, the linear flutter boundary defined using the doublet lattice theory, and the experimental flutter results from the Fall of 1989 and the Spring of 1991 wind-tunnel tests. Accounting for nonlinearities in the flow, by the application of the CAP-TSD code, is a clear improvement over the linear flutter predictions at transonic Mach numbers since the CAP-TSD prediction indicated the presence of a severe transonic flutter dip. The no-flutter track, shown in the figure, is the path, in terms of Mach number and dynamic pressure, through which the wind tunnel proceeded for which no flutter was encountered. This no-flutter track therefore defines a lower bound for the bottom of the experimental transonic flutter dip which disagrees with the bottom of the transonic flutter dip predicted using CAP-TSD. As a result, one of the goals of the present study was to investigate some of the possible causes of this discrepancy by modifying and improving specific elements of the analysis.

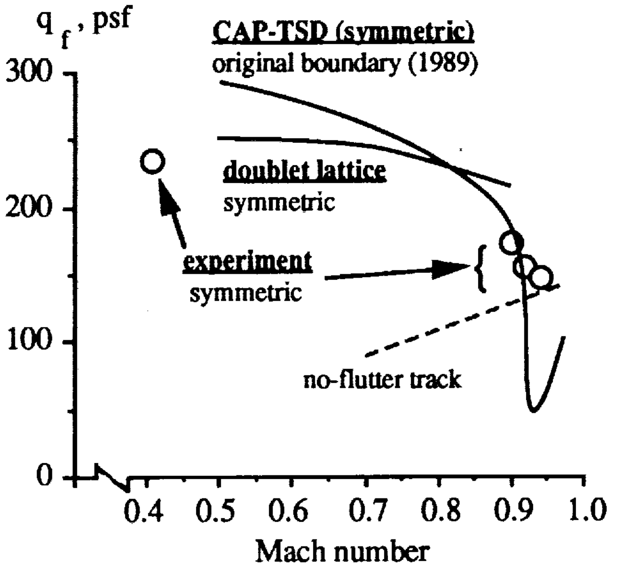

Fig. 6 Comparison of linear, nonlinear and experimental flutter boundaries for original mode shapes (Ref. 15)

Corrected tip store modeling- The first improvement to the analysis was the correction of an error in the modeling of the wing tip ballast store. The error consisted of a sign change in a portion of the slopes that geometrically define the tip store. The effect of this error was investigated and the resultant flutter boundary for the corrected wing tip ballast store model is presented in Fig. 7 along with the original, uncorrected flutter boundary presented in Fig. 6. At M_∞=0.5, the effect of the corrected tip store model was to reduce the flutter dynamic pressure from 290 to 259 psf with a change in flutter frequency from 10.70 to 11.20 Hz. At this Mach number there was no change in the flutter mechanism from the mechanism reported in Ref. 15, which consisted of a classical coalescence of the first-bending mode and the first-torsion mode. The flutter dynamic pressure dropped only slightly at M_∞=0.9 from 190 to 182 psf while at M_∞=0.93 the flutter dynamic pressure increased from 52 to 77 psf. The flutter dynamic pressure at M_∞=0.95 increased significantly from 81 to 133 psf. Again, the flutter mechanism at these three transonic Mach numbers was essentially the same as the mechanism reported in Ref. 15 for transonic Mach numbers, which consisted of a first-bending-dominated instability. The changes in flutter frequency at M_∞=0.9, 0.93, and 0.95 were, respectively, from 9.50 to 9.36 Hz, from 7.78 to 8.08 Hz, and from 8.07 to 8.83 Hz.

The corrected modeling of the wing tip ballast store therefore improved the flutter boundary by moving the flutter dynamic pressure in the direction of the experimental results at all Mach numbers. These results also indicate the sensitivity of the calculated flutter boundary to modeling of tip aerodynamics at subsonic and transonic conditions. For all of the results that follow, the corrected modeling of the wing tip ballast store has been included.

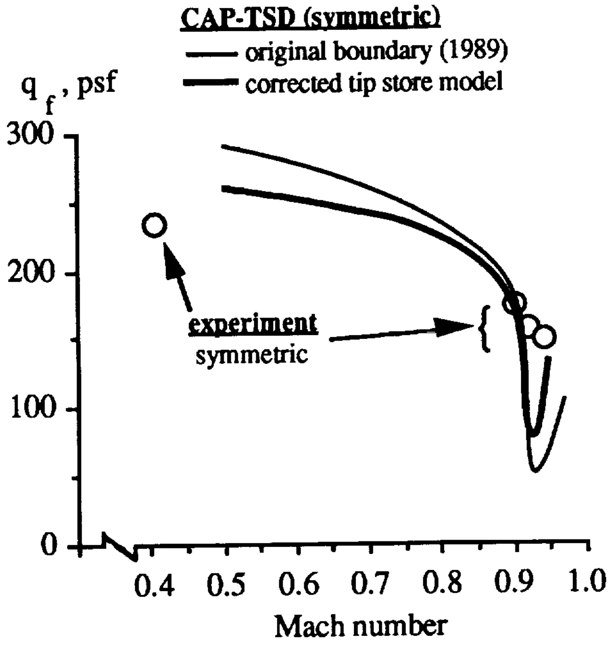

Fig. 7 The effect of the corrected tip store modeling on the symmetric flutter boundary using original structural model.

Updated mode shapes and frequencies- An updated and improved set of mode shapes and frequencies were obtained after the wind-tunnel test of 1989. The following improvements were made: a) refinements to the structural model based on experimental data and b) a denser set of structural points for improved mode shape definition, in particular around the control surface regions and the wing tip region of the AFW wind-tunnel model.

The flutter boundary obtained using the updated structural model is shown in Fig. 8 and compared to that obtained using the original structural model (corrected tip store model from Fig. 7). There is an increase in flutter dynamic pressure at M_∞=0.5 with the new structural model. The increase in flutter dynamic pressure is from 259 to 281 psf with a decrease in flutter frequency from 11.20 to 10.86 Hz. At M_∞=0.9, the flutter dynamic pressure increases from 182 to 203 psf with a slight change in flutter frequency from 9.36 to 9.44 Hz. The flutter dynamic pressure at M_∞=0.93 increases significantly from 77 to 103 psf with an increase in frequency from 8.08 to 8.32 Hz. For M_∞=0.95 the flutter dynamic pressure also increases significantly from 133 to 183 psf with an increase in flutter frequency from 8.83 to 9.33 Hz.

The updated structural model brings the computational results into closer agreement with experimental results at transonic Mach numbers greater than M_∞=0.9. But at M_∞=0.5 and 0.9 the comparison with experiment is degraded. A possible reason for this deficiency in the CAP-TSD prediction is that the current version of the code treats bodies such as the wing tip ballast store and fuselage as aerodynamic influences with no modal definition. Although the effect of a modally-defined fuselage on the flutter boundary may be minimal, the effect of a modally-defined wing tip ballast store is probably significant as can be seen by the sensitivity to changes in the modeling of the wing tip ballast store in Fig. 7. These effects should be investigated when a version of the CAP-TSD code becomes available that accounts for modal deformations of the fuselage and bodies and thus the contribution of these components to the generalized aerodynamic forces. Viscous effects, not accounted for in the current inviscid version of the code, also may have a significant effect on the subsonic and transonic flutter boundaries.

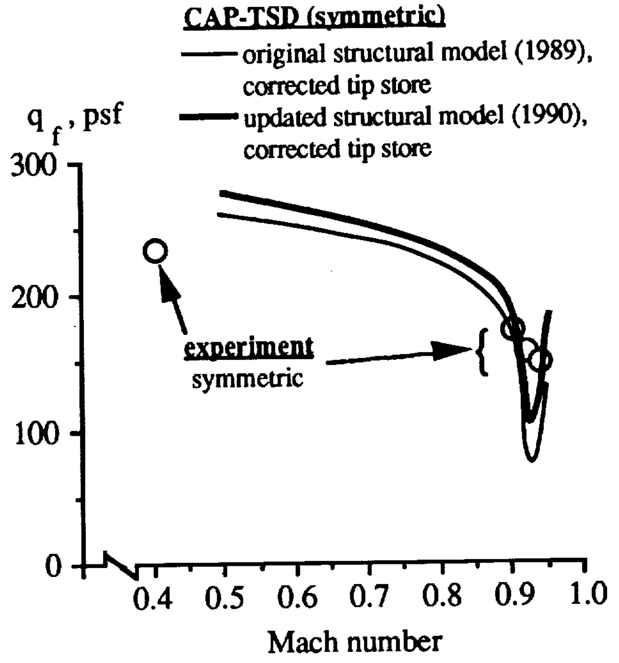

Fig. 8 Comparison of symmetric flutter boundaries for original (corrected) and updated structural models.

Vorticity and entropy corrections- The vorticity and entropy corrections defined in Ref. 19 and incorporated into current versions of the CAP-TSD code were applied with updated mode shapes and frequencies at M_∞=0.5, 0.9, 0.92, 0.93, and 0.95. These corrections typically reduce shock strength and shift the shock location forward. The resultant flutter boundary due to the implementation of these corrections is compared to the transonic portion of the flutter boundary for the updated structural model without vorticity and entropy corrections in Fig. 9. The effect of the corrections at M_∞=0.9 is minimal, lowering the flutter dynamic pressure from 203 to 200 psf and reducing the flutter frequency from 9.44 to 9.40 Hz. The effects of the corrections are significant at M_∞=0.93 where the flutter dynamic pressure increased from 103 to 126 psf with an increase in flutter frequency from 8.32 to 8.53 Hz. An interesting effect is noticed at M_∞=0.95 in that the flutter dynamic pressure is reduced from 183 to 130 psf and the flutter frequency drops from 9.33 to 8.60 Hz. The effect of the vorticity and entropy corrections therefore is significant in that it improves the correlation with experiment at the transonic Mach numbers evaluated. The inclusion of vorticity and entropy also tends to widen the rather steep and narrow transonic flutter dip previously computed (Figs. 6, 7, and 8).

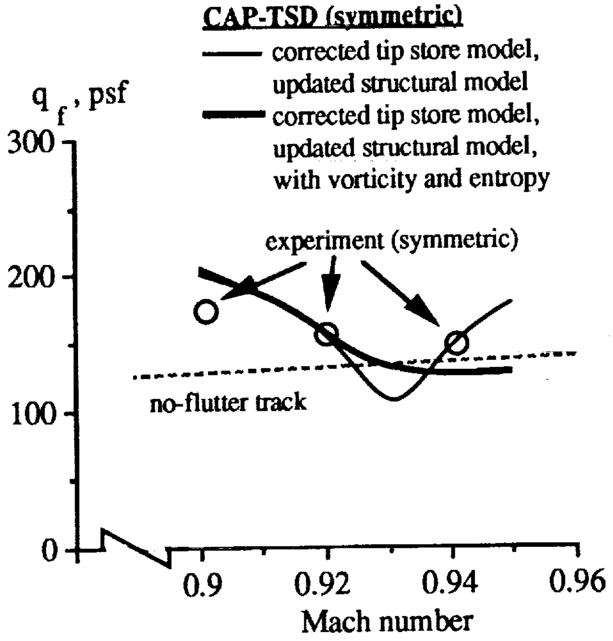

Fig. 9 Experimental and computational symmetric flutter boundaries with and without vorticity and entropy corrections.

In general, for symmetric motions, the effects of improved and updated analyses resulted in excellent agreement with experiment at transonic conditions while resulting in some degradation of the comparisons at M_∞=0.5 and 0.9. It is possible that accounting for the modal definition of the wing tip ballast store will provide some insight into this discrepancy. It is also interesting to note that the computational result at M_∞=0.92 is insensitive to the computational modifications and improvements described above and compares extremely well with experiment. At this Mach number, the calculated flutter dynamic pressure, for the vorticity and entropy case, for example, is 151 psf which differs only slightly from the experimental flutter value of 156 psf.

Dynamic Results - Antisymmetric motions

In order to generate antisymmetric aeroelastic responses, a full-span model of the AFW wind-tunnel model was generated. A progressive verification of the full-span model and of the capability of the CAP-TSD code for handling full-span aeroelastic analyses was deemed necessary before any antisymmetric flutter analyses were performed. This progressive verification proceeded as follows. First, a full-span, rigid and steady solution was compared to a semi-span, rigid and steady solution at the same Mach number. Lift and pitching moment coefficients for both cases were identical, thereby verifying the aerodynamic modeling of the full-span model and the accurate implementation of the symmetric boundary condition for the semi-span model. Second, static aeroelastic solutions were computed for both models using symmetric modes at a chosen Mach number and dynamic pressure. Again, the resultant lift and pitching moment coefficients, including static aeroelastic deformation of both models, were in exact agreement, verifying the modal definition of the full-span model. Finally, a full-span, symmetric dynamic analysis was compared to a semi-span, symmetric dynamic analysis resulting in identical transients, verifying the full-span model for dynamic analyses.

An important aspect of the antisymmetric flutter analyses was the necessary addition of symmetric mode shapes to the aeroelastic modeling along with the antisymmetric mode shapes. The reason for this is that since dynamic analyses are computed about converged static aeroelastic solutions and since static aeroelastic solutions are symmetric for a vehicle defined symmetrically about its centerline, antisymmetric dynamic analyses require the inclusion of symmetric modes as well. The computational model therefore consisted of ten symmetric modes needed for static aeroelastic solutions and ten antisymmetric modes needed for the dynamic aeroelastic solutions. These additional modes did not increase the computer time significantly as the finite-difference solution of Equation (1) dominated the CPU time.

Two antisymmetric flutter points have been computed for M_∞=0.5 and 0.9. Figure 10 is a comparison of the linear symmetric and antisymmetric flutter boundaries computed using doublet lattice aerodynamics and the updated set of mode shapes,[23] the nonlinear CAP-TSD symmetric flutter boundary for the updated set of mode shapes with vorticity and entropy corrections (Fig. 9), the nonlinear CAP-TSD antisymmetric flutter results at M_∞=0.5, 0.9 and the symmetric and antisymmetric experimental flutter points. Although the CAP-TSD predicted antisymmetric flutter dynamic pressure of 272 psf at M_∞=0.5 is significantly higher than the experimental value of 219 psf at M_∞=0.4, the CAP-TSD analyses indicate that the antisymmetric instability is lower in flutter dynamic pressure than the symmetric instability at M_∞=0.5 (dynamic pressure of 281 psf). This is consistent with the doublet lattice and experimental results. The discrepancy between the CAP-TSD results at M_∞=0.5 and the subsonic experimental flutter results may be due to the lack of modal definition of the wing tip ballast store and thus its contribution to the unsteady generalized forces in the CAP-TSD computations. The effect of a modally-defined wing tip ballast store on the subsonic and transonic CAP-TSD flutter boundaries still needs to be investigated. Furthermore, viscous effects have not been addressed by the analyses presented thus far and need to be investigated as well. The CAP-TSD antisymmetric flutter dynamic pressure at M_∞=0.9 is 245 psf, above the symmetric point at that Mach number. Determination of additional transonic antisymmetric flutter points using CAP-TSD continues.

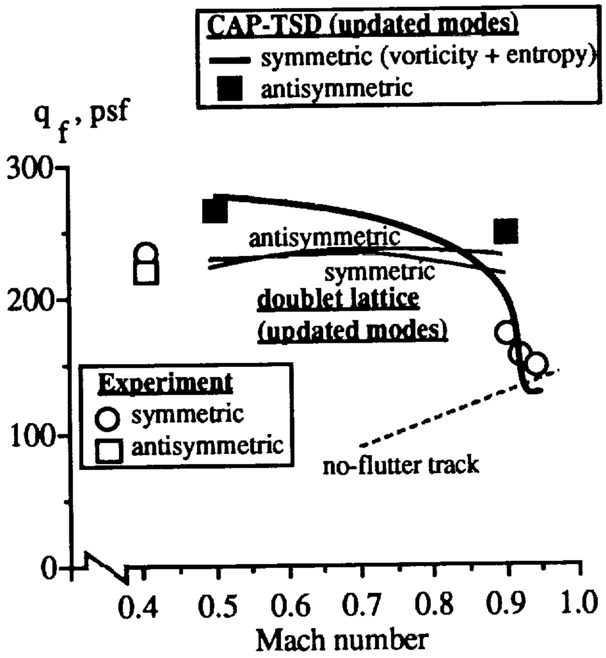

Fig. 10 Comparison of linear and nonlinear flutter boundaries for the updated symmetric (with vorticity and entropy) and antisymmetric structural model and experimental results.

CONCLUDING REMARKS

In this study, the calculated symmetric aeroelastic behavior of the AFW (Active Flexible Wing) wind-tunnel model using the CAP-TSD (Computational Aeroelasticity Code - Transonic Small Disturbance) code was updated. In addition, the full-span, antisymmetric aeroelastic capability of the code was evaluated and symmetric and antisymmetric results were compared with experimental flutter data.

The updated dynamic analyses consisted of modifications and improvements to key elements of the aeroelastic modeling. These modifications and improvements included a corrected aerodynamic modeling of the wing tip ballast store, an updated structural model, and the addition of vorticity and entropy corrections.

A static aeroelastic procedure previously developed was applied to an updated structural model. Results compared favorably with experimental data from a previous AFW wind-tunnel test. Static aeroelastic solutions therefore provided reasonable estimates of the static aeroelastic deformation of the wing. Dynamic analyses then were performed as perturbations about converged static aeroelastic solutions.

The corrected modeling of the wing tip ballast store resulted in improved correlation with subsonic and transonic symmetric experimental flutter points. The significant sensitivity of the aeroelastic analyses to changes in the modeling of the wing tip ballast store was revealed. The updated structural model improved the correlation with experiment at transonic Mach numbers but degraded the correlation with experiment at the subsonic condition. The addition of vorticity and entropy corrections provided further improvements in the correlation with experiment at transonic Mach numbers. This is an indication of the importance of including vorticity and entropy effects in the computations.

A full-span computational model of the AFW wind-tunnel model was generated and used for computing two antisymmetric flutter points at M_∞=0.5 and 0.9. Deficiencies in the correlation with experiment at M_∞=0.5 may be due to the lack of modal definition in the aerodynamics of the wing tip ballast store, which might have a significant effect on the generalized aerodynamic forces of the vehicle. Viscous effects, not accounted for in this inviscid version of the CAP-TSD code, may also play an important role in both the subsonic and transonic regimes. Determination of the rest of the antisymmetric flutter boundary using CAP-TSD continues.

ACKNOWLEDGEMENT

The authors would like to acknowledge B. Perry III of the Aeroservoelasticity Branch and S. R. Cole of the Configuration Aeroelasticity Branch for providing experimental flutter data.

REFERENCES

[1]Isogai, K. : On the Transonic-Dip Mechanism of Flutter of a Sweptback Wing. *AIAA Journal*, Vol. 17, No. 7, July 1979, pp. 793-795.

[2]Davis, S. S.; and Malcolm, G. N. : Experiments in Unsteady Transonic Flow. AIAA Paper No. 79-0769, AIAA/ASME/ASCE/AHS 20th Structures, Structural Dynamics, and Materials Conference, St. Louis, MO, April 4-6, 1979.

[3]Edwards, J. W.; and Malone, J. B. : Current Status of Computational Methods for Transonic Unsteady Aerodynamics and Aeroelastic Applications, NASA TM 104191, December 1991.

[4]Ballhaus, W. F.; and Bridgeman, J. O. : Numerical Solution Techniques for Unsteady Transonic Problems.

AGARD Report Number 679, Paper No. 16, March 1980.

[5]Wu, J. C. ; Kaza, K. R. V.; and Sankar, N. L. : A Technique for the Prediction of Airfoil Flutter Characteristics in Separated Flows. AIAA Paper No. 87-0910, Presented at the AIAA/ASME/ASCE/AHS 28th Structures, Structural Dynamics, and Materials Conference, Monterey, CA, April 6-8, 1987.

[6]Bendiksen, O. O.; and Kousen, K. : Transonic Flutter Analysis Using the Euler Equations. AIAA Paper No. 87-0911, Presented at the AIAA/ASME/ ASCE/AHS 28th Structures, Structural Dynamics, and Materials Conference, Monterey, CA, April 6-8, 1987.

[7]Shankar, V.; and Ide, H. : Unsteady Full Potential Computations Including Aeroelastic Effects. *Proceedings of the 5th International Conference on Numerical Methods in Laminar and Turbulent Flow*, Vol. 5, Part 2, Montreal, Canada, July 6-10, 1987.

[8]Borland, C. J.; and Rizzetta, D. P. : Nonlinear Transonic Flutter Analysis. *AIAA Journal*, Vol. 20, No. 11, November 1982, pp. 1606-1615.

[9]Yang, T. Y.; Guruswamy, P.; and Striz, A. G. : Application of Transonic Codes to Flutter Analysis of Conventional and Supercritical Airfoils. AIAA Paper No. 81-0603, Proceedings of AIAA Dynamics Specialist Conference, Atlanta, GA, April 9-10, 1981, pp. 332-342.

[10]Batina, J. T. : Efficient Algorithm for Solution of the Unsteady Transonic Small-Disturbance Equation. *Journal of Aircraft*, Vol. 25, No. 7, July 1988, pp. 598-605.

[11]Batina, J. T.; Seidel, D. A.; Bland, S. R.; and Bennett, R. M. : Unsteady Transonic Flow Calculations for Realistic Aircraft Configurations. *Journal of Aircraft*, Vol. 26, No. 1, January 1989, pp. 21-28.

[12]Bennett, R. M.; Bland, S. R.; Batina, J. T.; Gibbons, M. D.; and Mabey, D. G. : Calculation of Steady and Unsteady Pressures on Wings at Supersonic Speeds with a Transonic Small-Disturbance Code, *Journal of Aircraft*, Vol. 28, No. 3, March 1991, pp. 175-180.

[13]Bennett, R. M.;Batina, J. T.; and Cunningham,H. J. : Wing Flutter Calculations with the CAP-TSD Unsteady Transonic Small-Disturbance Program. *Journal of Aircraft*, Vol. 26, No. 9, September 1989, pp. 876 - 882.

[14]Perry, B. III; Cole, S. R.; and Miller, G. D.: A Summary of the Active Flexible Wing Program, AIAA Paper No. 92-2080, Presented at the Dynamics Specialists Conference, Dallas, Texas, April 16-17, 1992.

[15]Silva, W. A. ; and Bennett, R. M. : Predicting the Aeroelastic Behavior of a Wind-Tunnel Model Using Transonic Small-Disturbance Theory, ICAS Paper No. 90-1.1.1, Presented at the 17th International Council of the Aeronautical Sciences, Stockholm, Sweden, September 9-14, 1990.

[16]Yates, E. C. Jr.; Wynne, E. C. ; and Farmer, M. G. : Measured and Calculated Effects of Angle of Attack on the Transonic Flutter of a Supercritical Wing. NASA TM 83276, August 1982.

[17]Yates, E. C. Jr.; and Chu, L. : Static Aeroelastic Effects on the Flutter of a Supercritical Wing. NASA TM 89132, March 1987.

[18]Batina, J. T. : Unsteady Transonic Algorithm Improvements for Realistic Aircraft Applications. *Journal of Aircraft*, Vol. 26, No. 2, February 1989, pp. 131-139.

[19]Batina, J. T. : Unsteady Transonic Small-Disturbance Theory Including Entropy and Vorticity Effects. *Journal of Aircraft*, Vol. 26, No. 6, June 1989, pp. 531 - 538.

[20]Edwards, J. W.; Bennett, R. M.; Whitlow, W. Jr.; and Seidel, D. A. : Time-Marching Transonic Flutter Solutions Including Angle-of-Attack Effects. *Journal of Aircraft*, Vol. 20, No. 11, November 1983, pp. 899-906.

[21]Bennett, R. M.; and Desmarais, R. N. : Curve Fitting of Aeroelastic Transient Response Data with Exponential Functions. *Flutter Testing Techniques*, NASA SP-415, pp. 43-58, May 1975.

[22]Harder, R. L.; and Desmarais, R. N. : Interpolation Using Surface Splines. *Journal of Aircraft*, Vol. 9, No. 2, February 1972, pp. 189-191.

[23]Silva, W. A. ; Heeg, J. ; and Bennett, R. M. : Aeroelastic Modeling of the Active Flexible Wing Wind-Tunnel Model, In NASA CP 10065, Presented at the Fourth NASA Workshop on Computational Control of Flexible Aerospace Systems, Williamsburg, Virginia, July 11-13, 1990.

REPORT DOCUMENTATION PAGE

Form Approved
OMB No. 0704-0188

Public reporting burden for this collection of information is estimated to average 1 hour per response, including the time for reviewing instructions, searching existing data sources, gathering and maintaining the data needed, and completing and reviewing the collection of information. Send comments regarding this burden estimate or any other aspect of this collection of information, including suggestions for reducing this burden, to Washington Headquarters Services, Directorate for Information Operations and Reports, 1215 Jefferson Davis Highway, Suite 1204, Arlington, VA 22202-4302, and to the Office of Management and Budget, Paperwork Reduction Project (0704-0188), Washington, DC 20503.

1. AGENCY USE ONLY (*Leave blank*)

2. REPORT DATE
March 1992

3. REPORT TYPE AND DATES COVERED
Technical Memorandum

4. TITLE AND SUBTITLE
Further Investigations of the Aeroelastic Behavior of the AFW Wind-Tunnel Model Using Transonic Small Disturbance Theory

5. FUNDING NUMBERS
505-63-50-12

6. AUTHOR(S)
Walter A. Silva
Robert M. Bennett

7. PERFORMING ORGANIZATION NAME(S) AND ADDRESS(ES)
NASA Langley Research Center
Hampton, VA 23665-5225

8. PERFORMING ORGANIZATION REPORT NUMBER

9. SPONSORING/MONITORING AGENCY NAME(S) AND ADDRESS(ES)
National Aeronautics and Space Administration
Washington, DC 20546-001

10. SPONSORING/MONITORING AGENCY REPORT NUMBER
NASA TM-107576

11. SUPPLEMENTARY NOTES
Will be presented at the Dynamics Specialists Conference, April 16-17, 1992, Dallas, Texas

12a. DISTRIBUTION/AVAILABILITY STATEMENT
Unclassified-Unlimited

Subject Category 02

12b. DISTRIBUTION CODE

13. ABSTRACT (*Maximum 200 words*)

The CAP-TSD (Computational Aeroelasticity Program - Transonic Small Disturbance) code, developed at the NASA Langley Research Center, is applied to the Active Flexible Wing wind-tunnel model for prediction of transonic aeroelastic behavior. A semi-span computational model is used for evaluation of symmetric motions, and a full-span model is used for evaluation of antisymmetric motions. Static aeroelastic solutions using CAP-TSD are computed. Dynamic (flutter) analyses then are performed as perturbations about the static aeroelastic deformations and presented as flutter boundaries in terms of Mach number and dynamic pressure. Flutter boundaries that take into account modal refinements, vorticity and entropy corrections, antisymmetric motions and sensitivity to the modeling of the wing tip ballast stores also be presented and compared with experimental flutter results.

14. SUBJECT TERMS
Transonic Flutter
Transonic Small Disturbance
CAP-TSD
Active Flexible Wing

15. NUMBER OF PAGES
11

16. PRICE CODE
A03

17. SECURITY CLASSIFICATION OF REPORT
Unclassified

18. SECURITY CLASSIFICATION OF THIS PAGE
Unclassified

19. SECURITY CLASSIFICATION OF ABSTRACT
Unclassified

20. LIMITATION OF ABSTRACT

NSN 7540-01-280-5500

Standard Form 298 (Rev. 2-89)